UCRL-TR-226690

LAWRENCE LIVERMORE NATIONAL LABORATORY

Experimental Validation of LLNL Finite Element Codes for Nonlinear Seismic Simulations (Progress, Year 1 of 2)

S.W. Alves, C.R. Noble
Structural and Applied Mechanics Group

September 2006

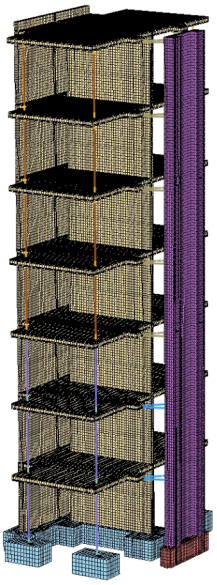

This work was performed under the auspices of the U.S. Department of Energy by University of California, Lawrence Livermore National Laboratory under Contract W-7405-Eng-48.

Table of Contents

List of Figures

List of Tables

1.0 Introduction

Shake table tests were performed on a full-scale 7-story slice of a reinforced concrete building at UC San Diego between October 2005 and January 2006. The tests were performed on the NEES Large High-Performance Outdoor Shake Table (LHPOST) at the Engelkirk Structural Engineering Center of UCSD. The structure was subjected to four uniaxial earthquake ground motions of increasing amplitude. The accelerations measured at the base of the structure and the measured roof displacements have been provided by UCSD. Details of the building construction have also been provided by UCSD. The structure is shown in Figure 1.

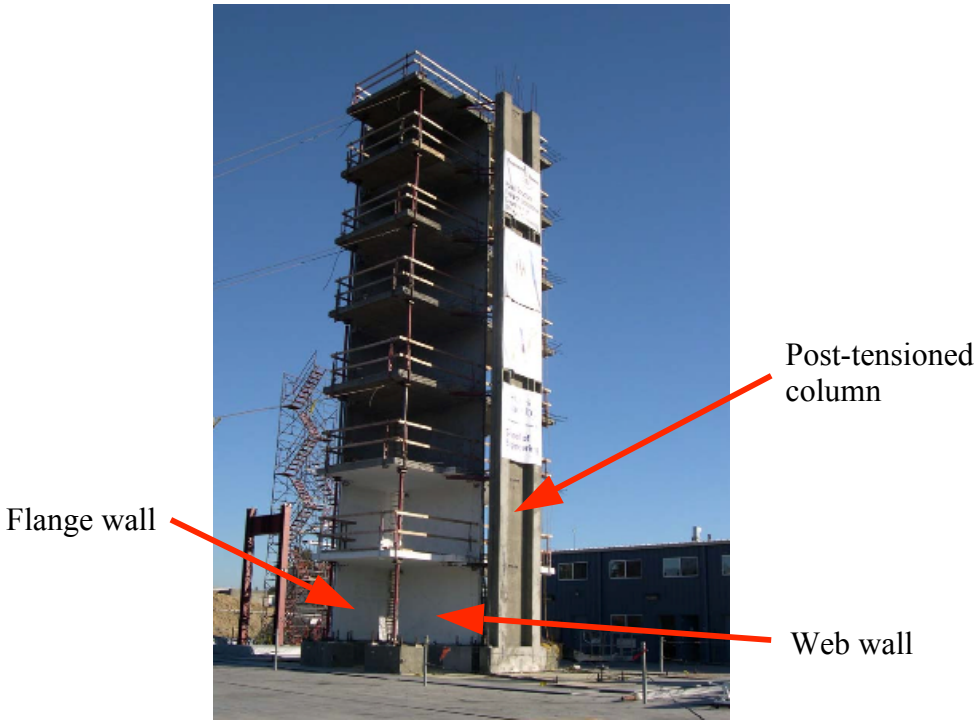

Figure 1. Test structure at UCSD

The measured response of this structure was used to assess the capability of the homogenized rebar model in DYNA3D/ParaDyn [1,2] to simulate the seismic response of reinforced concrete structures. The homogenized rebar model is a composite version of the Karagozian & Case concrete model [3]. Work has been done to validate this material model for use in blast simulations, but seismic simulations require longer durations. The UCSD experiment provides full-scale data that can be used to validate seismic modeling capabilities.

2.0 Material Properties and Boundary Conditions

The structure consists of a main shear wall (the web wall), a wall perpendicular to the web wall (the flange wall), concrete slabs at each floor, a post-tensioned column that reduces torsion, and four gravity columns supporting the slabs. The floor slabs connect the web wall and the flange wall, but the connection between the walls is double-hinged. The post-tensioned column is connected to the structure by braces at each floor. The entire structure is situated on a concrete

foundation that is anchored to the shake table platen. The input motion was applied along the direction parallel to the web wall. UCSD provided properties for the concrete and steel that were tested during construction.

The compressive strength, elastic modulus and ultimate strain for the concrete are summarized in Table 1. A representative stress-strain curve defining these values and the concrete placement are shown in Figure 2. Note that the concrete properties for the foundation and the first 4 inches of the flange wall at floors 2-7 were not provided. The compressive strength and elastic modulus for the concrete used in the finite element analyses for the walls, the floor slabs and the foundation are averaged from c3, c5, c7, c9, c11, c13 and c15 (f_c' = 5.87 ksi and E_c = 4350 ksi). The compressive strength and elastic modulus for the concrete in the post-tensioned column and its foundation are averaged from c17 and c18 (f_c' = 5.54 ksi and E_c = 4300 ksi). The unit weight of the concrete is assumed to be 150 lbs/ft^3 (0.0868 lbs/in^3), and the Poisson's ratio is assumed to be 0.2.

Table 1. Concrete properties supplied by UCSD

Concrete tabulated material properties							
concrete placement		**fc' (ksi)**	**fc' avg (ksi)**	**Ec (ksi)**	**Ec avg (ksi)**	**εcu**	**εcu avg**
c2	specimen1	8.00	7.87	3415	3349	-0.00291	-0.00281
	specimen2	7.74		3282		-0.00271	
c3	specimen1	5.30	5.43	4019	3549	-0.00244	-0.00269
	specimen2	5.56		3080		-0.00294	
c5	specimen1	5.58	5.70	3875	3771	-0.00202	-0.00229
	specimen2	5.81		3666		-0.00256	
c7	specimen1	6.00	6.11	4626	5053	-0.00237	-0.00214
	specimen2	6.22		5480		-0.00192	
c9	specimen1	5.86	6.03	4491	4380	-0.00212	-0.00236
	specimen2	6.21		4269		-0.00261	
c11	specimen1	5.62	5.80	4121	4191	-0.00214	-0.00225
	specimen2	5.99		4262		-0.00236	
c13	specimen1	5.68	5.78	4886	4661	-0.00226	-0.00233
	specimen2	5.88		4435		-0.00239	
c15	specimen1	6.26	6.25	4762	4864	-0.00209	-0.00210
	specimen2	6.23		4965		-0.00211	
c17	specimen1	5.66	5.62	4439	4194	-0.00249	-0.00234
	specimen2	5.59		3949		-0.00220	
c18	specimen1	5.40	5.45	4903	4398	-0.00192	-0.00220
	specimen2	5.51		3894		-0.00247	

The yield strength, ultimate strength, yield strain and ultimate strain for the rebar are summarized in Table 2, and a representative stress-strain curve defining these values is shown in Figure 3. The yield strength, ultimate strength and ultimate strain for all steel in the finite element model are averaged from b1 through b11 (f_y = 66.5 ksi, f_{su} = 107 ksi, ε_{su} = 0.102). The unit weight of steel is assumed to be 0.283 lbs/in^3, and the Poisson's ratio is assumed to be 0.29. The elastic modulus of the steel is assumed to be 29e6 psi.

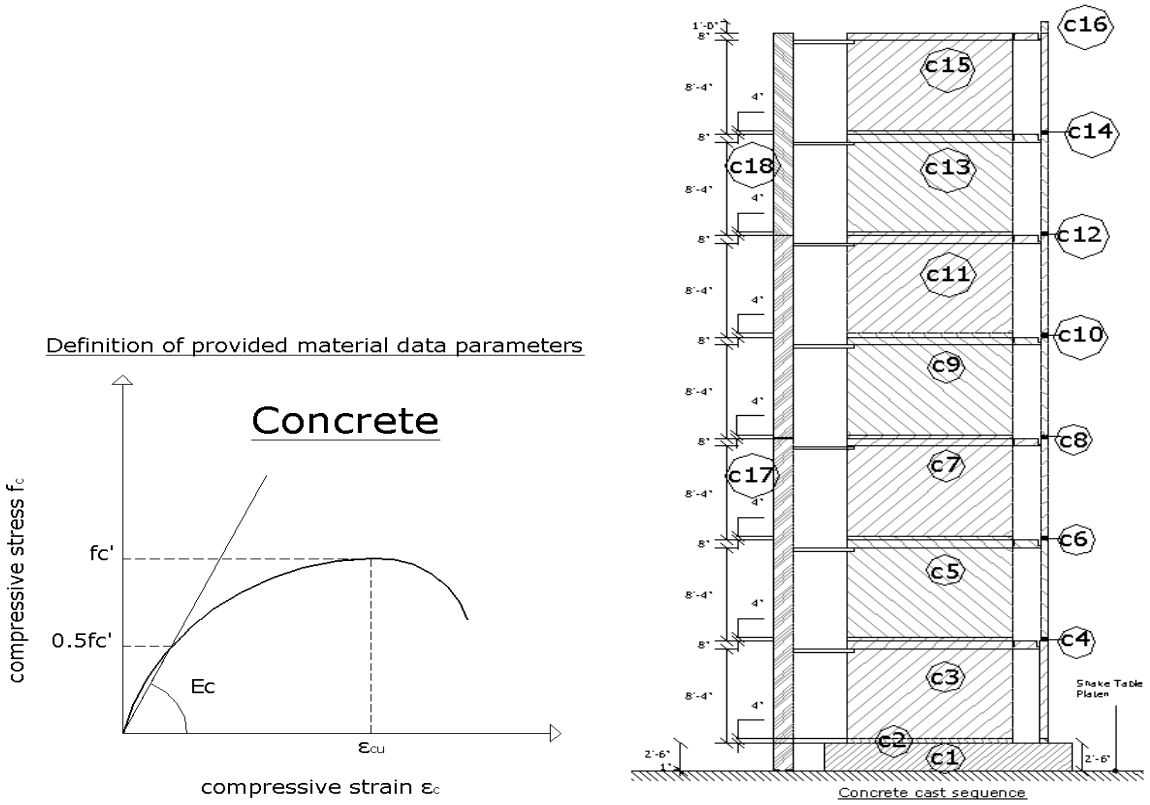

Figure 2. Representative concrete stress-strain curve for properties supplied by UCSD (left), and schematic of concrete specimen locations (right)

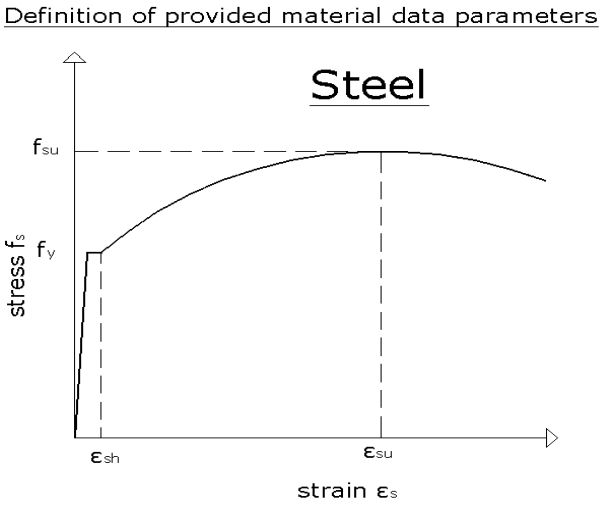

Figure 3. Representative steel stress-strain curve for properties supplied by UCSD

Table 2. Rebar properties supplied by UCSD

Reinforcing Steel tabulated meterial properties					
bar name		**fy (ksi)**	**fsu (ksi)**	**εsh**	**εsu**
b1	spec1	65.2	108.6	0.0060	0.0988
	spec2	64.8	109.0	-	0.1034
	spec3	65.7	109.2	0.0047	0.1004
	avg	**65.2**	**108.9**	**0.0054**	**0.1009**
b2	spec1	63.4	103.2	0.0081	0.1121
	spec2	62.9	102.9	0.0072	0.1090
	spec3	63.1	103.0	0.0069	0.1077
	avg	**63.1**	**103.0**	**0.0074**	**0.1096**
b3	spec1	66.1	101.0	0.0075	0.1158
	spec2	65.6	101.0	0.0081	0.1098
	spec3	-	-	-	-
	avg	**65.9**	**101.0**	**0.0078**	**0.1128**
b4	spec1	69.3	111.1	0.0074	0.1158
	spec2	68.9	111.1	0.0083	0.1075
	spec3	-	-	-	-
	avg	**69.1**	**111.1**	**0.0079**	**0.1117**
b5	spec1	65.7	112.6	0.0071	0.1077
	spec2	65.6	112.4	0.0068	0.1028
	spec3	-	-	-	-
	avg	**65.7**	**112.5**	**0.0070**	**0.1053**
b6	spec1	71.4	114.0	0.0057	0.1001
	spec2	71.7	113.6	0.0053	0.1060
	spec3	71.6	113.6	0.0046	0.1079
	avg	**71.6**	**113.7**	**0.0052**	**0.1046**
b7	spec1	66.5	98.0	0.0061	0.0406
	spec2	65.6	107.5	0.0052	0.1064
	spec3	67.0	107.7	0.0049	0.1039
	avg	**66.4**	**104.4**	**0.0054**	**0.0836**
b8	spec1	66.3	105.2	0.0091	0.1146
	spec2	66.0	105.2	0.0086	0.1224
	spec3	65.7	105.0	0.0080	0.1136
	avg	**66.0**	**105.1**	**0.0086**	**0.1169**
b9	spec1	63.7	102.5	0.0090	0.1154
	spec2	62.9	101.8	0.0078	0.1102
	spec3	64.0	102.1	0.0094	0.1036
	avg	**63.5**	**102.1**	**0.0087**	**0.1098**
b10	spec1	60.3	98.4	-	0.0889
	spec2	66.3	108.5	-	0.0941
	spec3	66.5	108.8	-	0.0903
	avg	**64.4**	**105.2**	**-**	**0.0911**
b11	spec1	71.0	109.9	0.0052	0.0905
	spec2	70.9	109.4	0.0053	0.0952
	spec3	70.9	107.0	0.0055	0.0545
	avg	**70.9**	**108.7**	**0.0053**	**0.0800**

The gravity columns (Figure 4) consist of high-strength Dywidag Threadbar rods that are embedded in 4" diameter steel pipe with grout between the rod and the pipe. The Dywidag Threadbar rods have an elastic modulus of 29.7e6 psi. At levels 1-3, the columns are 1.75" diameter rod and Extra Strong steel pipe; and at levels 4-7, the columns are 1.375" diameter rod and Standard steel pipe. There were ball joints at both ends. The gravity columns were designed to remain elastic, so they are modeled as elastic in the finite element analyses.

Figure 4. End connection of a gravity column

The braces connecting the post-tensioned column to the structure (Figure 5) are L-section beams. At levels 1-2, the braces are L4x4x3/8; and at levels 3-7, the braces are L3x3x5/16. Like the gravity columns, the braces were designed to remain elastic, so they are modeled as elastic.

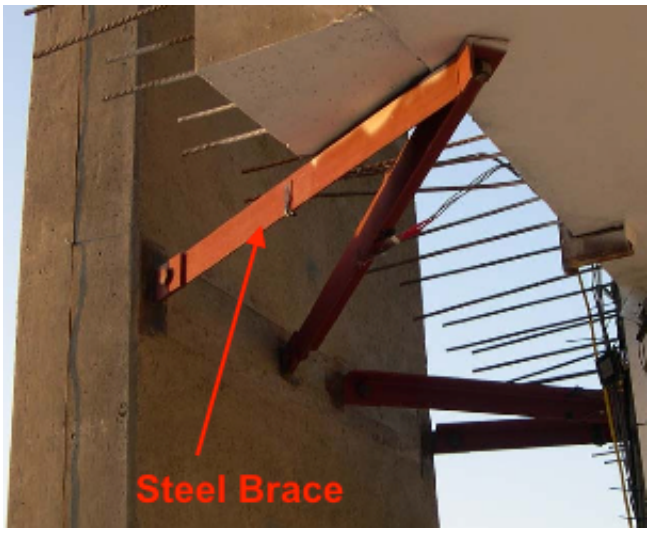

Figure 5. Braces connecting the post-tensioned column to a floor slab

The post-tensioned column was post-tensioned with two 1.25" diameter high-strength Dywidag rods. The force in each rod was 110 kips. The column was designed to rock at its base in the direction of the ground motion. This was accomplished by including a hinge at the base of the foundation for the column.

The input ground motions were provided as accelerations that were measured at the top of the foundation. Before using these raw acceleration records as input to a finite element model, they

were filtered to remove drifts caused by measurement noise (Larry Hutchings, personal communication, April 11, 2006). The resulting acceleration histories for each of the four earthquakes are shown in Figure 6. In order to include the flexibility from the foundation in the simulations, the foundation was included in the model and the ground acceleration was applied at the base of the foundation. The rationale is that while the motion is not identical at the top and the base of the foundation, it is very similar.

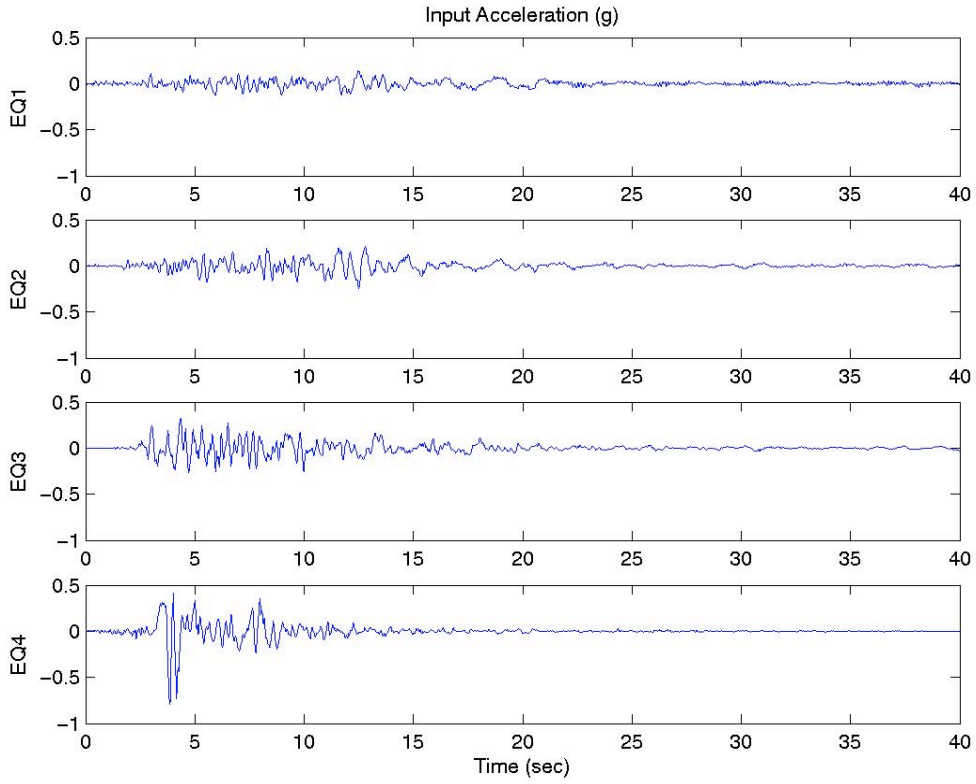

Figure 6. Acceleration time histories that are applied to the finite element model

Other modeling assumptions are summarized below:

- The ends of the gravity columns and the braces are modeled as fixed, as opposed to pinned. In the actual structure, the gravity columns had ball joints at both ends and the braces would most accurately be described as pinned about one axis and fixed about the other two axes at both ends. However, both the braces and columns are modeled as fixed at the ends to reduce the effects from stress concentrations and minimize the contribution to hourglass modes. The significance of this is expected to be small for the overall behavior of the structure.
- There is slackness at the connections of the gravity columns (0.08 inches at levels 1-3 and 0.4 inches at levels 4-7) that must be overcome before the columns can take tension. This slackness is neglected in the model. Again, the significance of this is expected to be small for the overall behavior of the structure.

- The sections of the gravity columns that are embedded in steel pipe and grout are modeled as beams that carry axial loads as if they were only the Dywidag Threadbar rod, but the entire composite beam carries bending loads. The rationale is that the axial load cannot be transmitted from the rod to the grout to a significant degree.
- Before the structure was subjected to the fourth earthquake motion, the connection between the bracing and the first level slab was slotted in the direction of motion. This is ignored in the model, because the overall behavior of the structure is not expected to be affected significantly.
- The post-tensioned column was fabricated as three precast pieces. No reinforcement crossed the joints between the pieces. In the model, the homogenized rebar is spread out over the entire height of the column and no gap in the rebar is modeled. This assumption is not expected to affect the response of the rest of the structure significantly.
- There is a protection system employing guy wires attached to the structure and anchored to the ground that would pull the structure away from the control building in the event of a collapse. The effect of these wires is insignificant because the stiffness/mass of the wires is small compared to the stiffness/mass of the structure, so the wires are neglected in the finite element model.
- For modeling purposes, the shake table platen is assumed to be rigid with no rotation. The flexibility and rotation of the platen were estimated to have a negligible effect on the response of the structure (less than 5% of the roof deflection).

3.0 NIKE3D Analyses

A linear model of the structure was generated without the rebar included. With gravity applied to the structure and the pressure from the post-tensioned rods applied at the top and the base of the column, a static analysis was run in NIKE3D [4]. The concrete was defined with the elastic modulus of the concrete that was determined from the data provided by UCSD. The natural frequencies and mode shapes of the structure were determined from an eigen-analyis of the structure. The first mode of the structure is torsional with a frequency at 2.17 Hz. The second mode is the first-order cantilever mode of the structure with a frequency at 2.65 Hz. The mode at 2.65 Hz should be the dominant mode of the earthquake response since the building is excited uniaxially in the direction of motion for that mode. The mode shapes for these two modes are shown in Figure 7.

Some sensitivity tests were done with this linear model. The effects on the natural frequencies of the first two modes are summarized in Table 3. The significance of fixing the ends of the gravity columns and the braces was tested by modifying the model to have pinned connections. For reasons that will be explained in the following sections, the effects of modifying the stiffness and mass of certain components of the model were also investigated. The modifications were:

- Decrease the elastic modulus of the gravity columns and braces by a factor of 10 (Case 1)
- Increase the mass of floor 7 by 100% (Case 2)
- Increase the mass of floor 7 by 100% and the rest of the building mass by 25% (Case 3)
- Increase the mass of the entire building by 20%, increase the masses of floors 1-6 by another 50% and increase the mass of floor 7 by another 100% (Case 4)
- Increase the mass as in Case 4 and decrease the elastic modulus to 3500 ksi (Case 5)

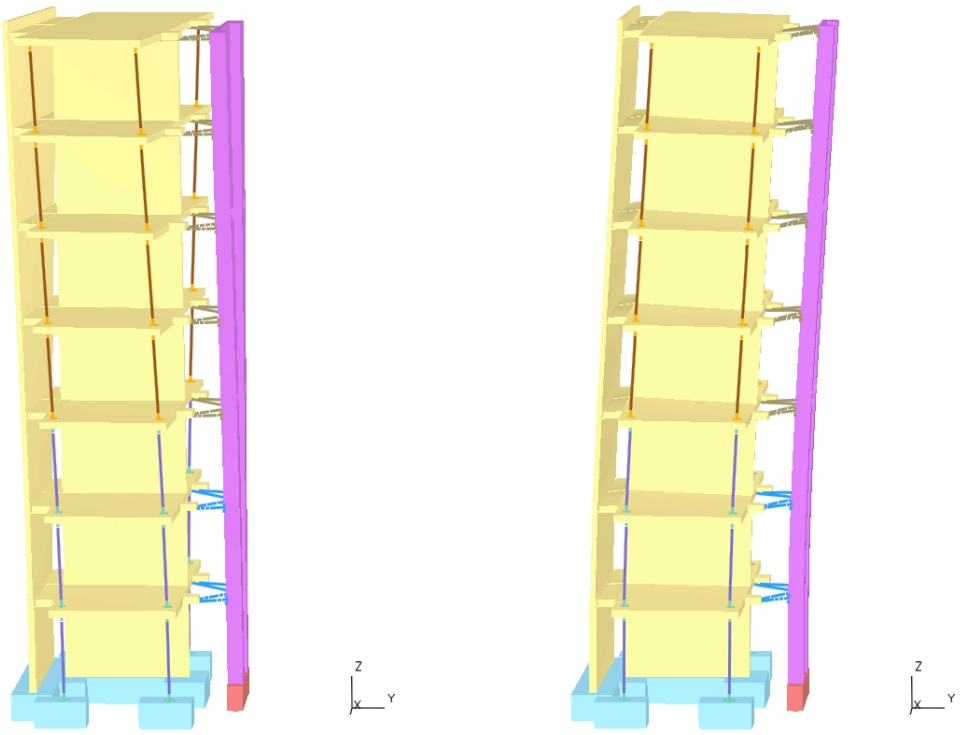

Figure 7. First torsional mode shape at 2.17 Hz (left), and first cantilever mode shape at 2.65 Hz (right)

Table 3. Natural frequencies of the first torsional and first cantilever modes

	Torsional Mode	Cantilever Mode
Base Case	2.17 Hz	2.65 Hz
Pinned Connection	2.16 Hz	2.63 Hz
Case 1	2.07 Hz	2.59 Hz
Case 2	1.95 Hz	2.39 Hz
Case 3	1.87 Hz	2.25 Hz
Case 4	1.67 Hz	2.04 Hz
Case 5	1.51 Hz	1.84 Hz

The small difference that occurs when the connections are pinned instead of fixed illustrates the insignificance of the assumption of fixed connections. In fact, reducing the stiffness of the gravity columns and braces by a factor of 10 (essentially removing them) causes only a minor effect on the overall stiffness of the structure. The various increases in mass throughout the structure investigate the effects of extreme variations to bound the effects of possible mass variations. The last case also decreases stiffness to include that effect in the bounding study. These results will be discussed further in following sections.

4.0 ParaDyn Analyses

4.1 Linear Model

The finite element mesh of the model that was generated for NIKE3D was refined to be able to capture the characteristics of the rebar. This refined model was run in DYNA3D/ParaDyn [1,2]. However, before running analyses with the rebar and a nonlinear concrete model, linear analyses with the same material properties as the NIKE3D model were run for all four earthquake ground motions. The model is illustrated in Figure 8. Mass proportional damping is used to attain 3% of critical damping at approximately 2.6 Hz. Note that these linear analyses were set up with pinned connections at the gravity columns and braces. This difference should have a negligible significance.

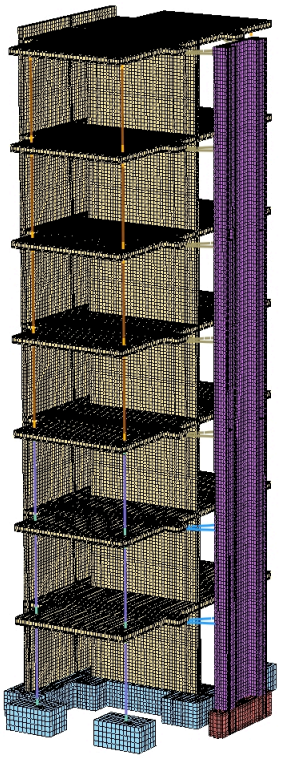

Figure 8. Finite element model of the structure used for linear simulations in ParaDyn

The modeled roof displacement is compared to the measured roof displacement for all four earthquakes in Figure 9. Notice that the modeled displacement significantly underestimates the measured displacement for all four earthquakes. The peak displacements are compared in Table 4. Also, the roof oscillated at a much lower frequency during the experiment than the model predicts. This is not surprising, because the model is linear. Thus, the model cannot be damaged like the actual structure. It can be seen from the roof displacements recorded during the experiment that each earthquake progressively damaged the structure, because the frequency of oscillation decreases. Since the model is linear, the frequency of oscillation for the simulated roof displacement histories is the same for all four earthquakes, just above 2.5 Hz. (Recall that

the natural frequency of the first cantilever mode is 2.63 Hz with pinned connections.) However, the discrepancy between the simulated and measured displacements for the first earthquake is larger than would be expected considering the amplitude of the motion. Perhaps, the actual structure is already in a significantly nonlinear state at the start of the first earthquake. Settling of the structure and low-amplitude white noise input tests performed prior to the earthquake tests could have caused concrete damage even before the first earthquake test was run. Other reasons for the discrepancy are also possible and this will be discussed further in the following sections.

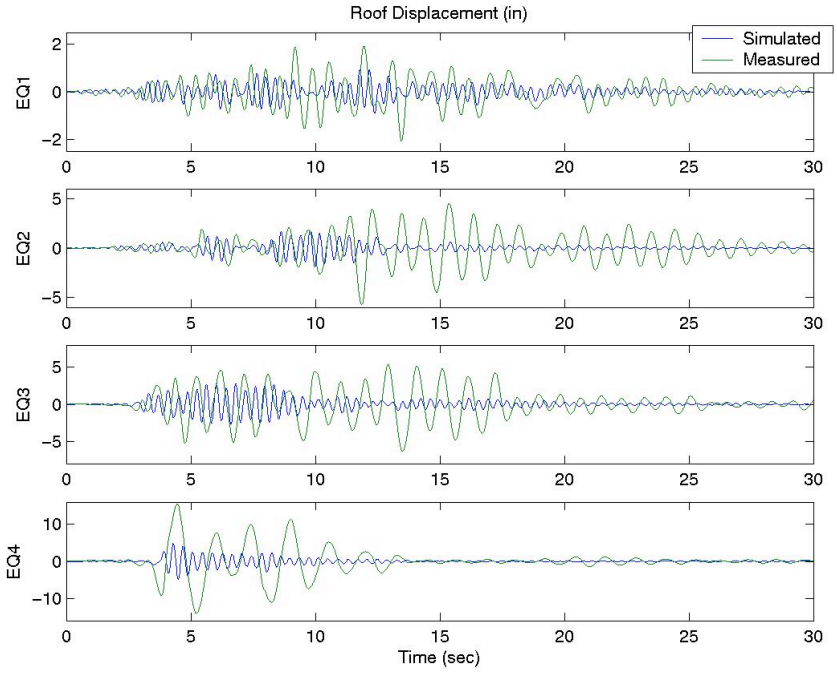

Figure 9. Roof displacements computed from the linear model for four earthquake ground motions compared to the measured roof displacements

Table 4. Peak values of the simulated (linear model) and measured roof displacements for four earthquake ground motions

	Peak Simulated Displacement	Peak Measured Displacement
EQ1	0.92 in	2.05 in
EQ2	1.91 in	5.75 in
EQ3	2.81 in	6.29 in
EQ4	4.92 in	15.55 in

4.2 Nonlinear Model

4.2.1 Concrete/Rebar Material Model

The concrete model used in the simulations is the DTRA concrete model developed by Karagozian & Case, which is material type 45 in DYNA3D [1,3]. This concrete model

decouples the volumetric and deviatoric responses, and it uses an equation of state to define pressures and unloading bulk moduli as functions of volumetric strain. There are three independent failure surfaces that define the plastic behavior of the concrete. The failure surfaces are based on the second invariant of the deviatoric stress tensor. The material is linear up to the yield failure surface. Then the material transitions to the maximum failure surface, and after reaching the maximum strength the material softens until reaching the residual failure surface. There is a damage parameter associated with these failure surfaces. Until yield is reached, the damage parameter is 0. The value is 1 at the maximum surface, and 2 when the residual surface is reached. Material type 65 in DYNA3D is an update of material type 45 that generates all of the parameters for material type 45 using only the unconfined compressive strength of the concrete [1].

The homogenized rebar model used in the simulations is material type 66 in DYNA3D [1,3]. The DTRA concrete model (type 45) is used to model the concrete, and it is augmented with a rebar model that can have rebar in up to three arbitrary directions with differing properties. Strain-rate dependence, work hardening and tensile failure are included in the rebar model. Only axial response is considered in the rebar. The homogenized rebar model is attractive to use because of its relative efficiency in computation and mesh generation compared to explicitly modeling the rebar with brick or beam elements.

4.2.2 Problems Encountered with DYNA3D

A nonlinear analysis of the structure requires that the four earthquake motions be applied in succession in order to account for accumulated nonlinear effects. However, there is an instability in the DTRA concrete model that caused the nonlinear analysis to stop prematurely. A singularity exists in the model formulation that leads to very large local deformations and element inversion. Up to the point where the analysis stops, the response of the structure is not affected by the singularity so the results can still be used.

Two other problems in DYNA3D/ParaDyn hampered the analysis effort. If material type 65, the update to material type 45, is used in the analysis, the response of the structure becomes noisy. The problem can be avoided by using material type 45. Also, the stress initialization feature does not function correctly for the new element architecture. To work around this, the old element architecture can be used or the entire analysis can be run in one step without any intermediate stress initialization. Both of these errors in the code need to be tracked down and corrected.

Finally, with the connection of beam elements to under-integrated solid elements and long analysis times, hourglassing can become very significant. If viscous hourglass control is used, the hourglass modes can dominate. Thus, the hourglass control was changed to stiffness form.

4.2.3 Comparison to Experiment

Prior to running the nonlinear analysis, the finite element model was modified to have a plane of symmetry (Figure 10). While the lowest mode of the structure is torsional, the earthquake loading will not excite this mode so the symmetry model is used for computational efficiency.

Concrete properties were obtained by inputting the compression strength of the concrete into material type 65. The parameters output from material type 65 are used in input to material types 45 and 66. The compression strength was determined from the data provided by UCSD (f_c' = 5.87 ksi for the building and f_c' = 5.54 ksi for the post-tensioned column, see Section 2.0). The tensile strengths were 514.1 psi and 494.7 psi for the building and post-tensioned column, respectively. Based on the initial bulk moduli, the elastic modulus of the concrete is very close to the values used in the linear analyses (E_c = 4350 ksi for the building and E_c = 4300 ksi for the post-tensioned column). Steel properties for the rebar are described in Section 2.0. Like the linear model, 3% of critical damping at 2.6 Hz is attained by mass proportional damping.

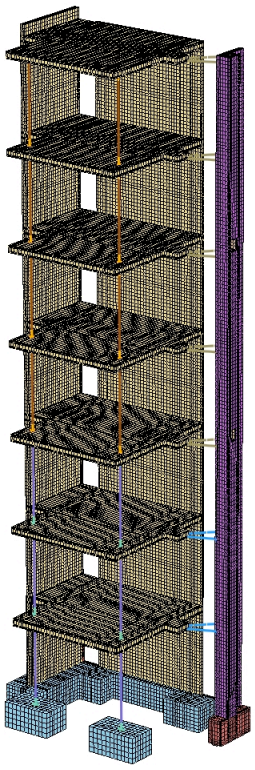

Figure 10. Half-symmetry finite element model of the structure used for nonlinear simulations in ParaDyn

The analysis could only be run through the first earthquake ground motion before the singularity discussed in Section 4.2.2 caused the analysis to stop. Like the linear model, the simulated roof displacement significantly underestimates the measured roof displacement and the model produces a much stiffer system than the actual structure. The simulated displacement is compared to the measured displacement in Figure 11. The simulated displacement from the linear model is also included for comparison. Notice how similar the nonlinear model is to the linear model at the start before inelastic behavior becomes significant. Also, notice that the nonlinear model is still far too stiff. This is further illustrated by the frequency response curves shown in Figure 12.

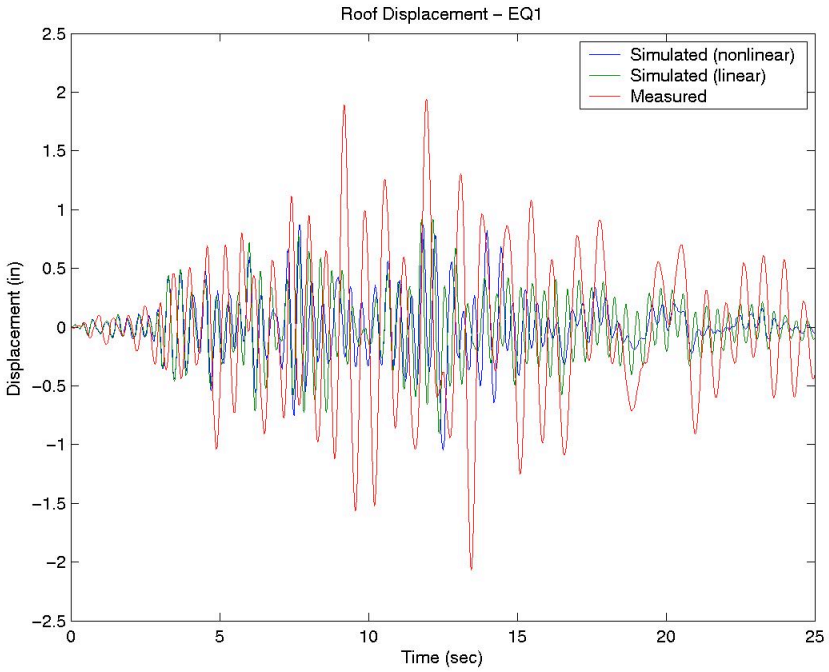

Figure 11. Roof displacements computed from the nonlinear and linear models for the first earthquake ground motion compared to the measured roof displacement

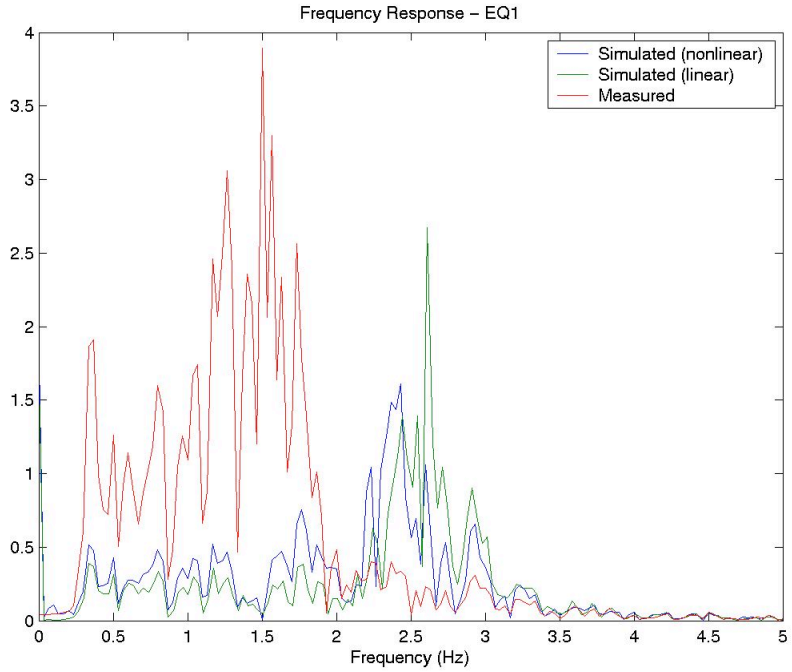

Figure 12. Frequency response curves of the roof displacements computed from the nonlinear and linear models for the first earthquake compared to the frequency response of the measured roof displacement

The relatively low stiffness of the actual structure does not appear to be a result of damage that occurred during the first earthquake. The natural frequency of the structure is low from the beginning of the ground motion. As discussed in Section 4.1, settling under gravity and the white noise tests may have already significantly damaged the structure, which is not captured by the model, but that alone cannot explain the discrepancies. Figure 13 shows that the model had actually incurred a substantial amount of damage near its base midway through the earthquake. The effect of this damage on the modeled response is not nearly enough to approach the measured response. Recall that the damage parameter is defined such that a value of 0 corresponds to no damage, 1 corresponds to reaching the maximum surface, and 2 corresponds to reaching the residual surface.

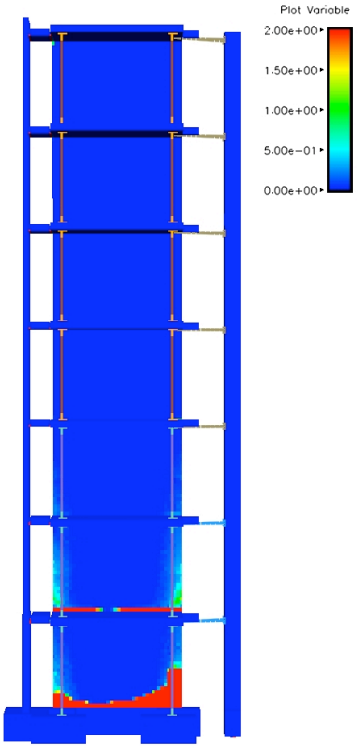

Figure 13. Plot of the concrete damage parameter throughout the nonlinear model midway through the first earthquake

The nonlinear model was also run with pinned connections for the gravity columns and braces. As predicted, the effect on the overall behavior of the structure is insignificant. This is illustrated in Figure 14 by a comparison of the roof displacements simulated with pinned and fixed connections.

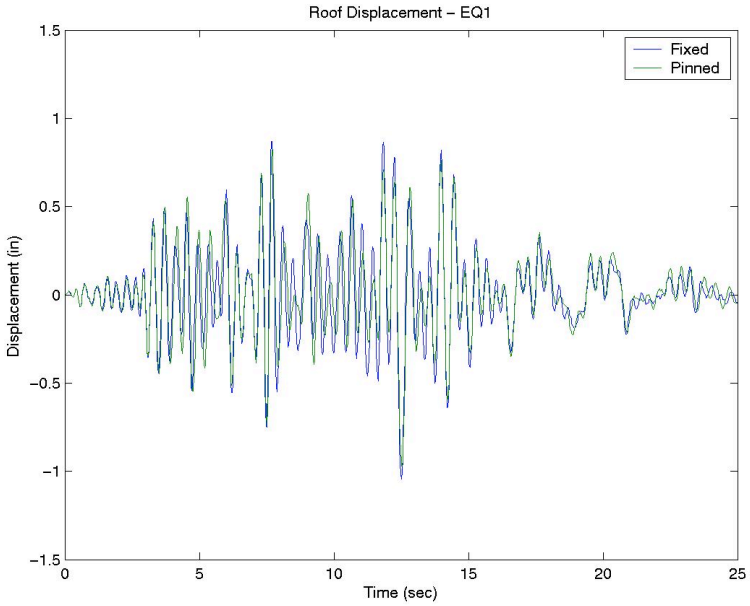

Figure 14. Comparison of the roof displacement computed for the first earthquake with fixed and pinned connections at the ends of the gravity columns and braces

4.2.4 Model Variations

Three more test analyses were run with variations in the model. First, the homogenized rebar was removed from the model so that the entire structure was concrete. Second, the homogenized rebar was put back into the model, but a weaker concrete was used. Stress-strain curves for the two concrete models are compared in Figure 15. Third, the original model was used except the mass proportional damping was removed. With the mass proportional damping removed, an element inverts shortly after the completion of the first earthquake and the analysis is stopped. However, with no rebar and weaker concrete, the singularity in the concrete material formulation is never reached so both of those analyses ran to the completion of all four earthquakes. The reason for this is not fully understood.

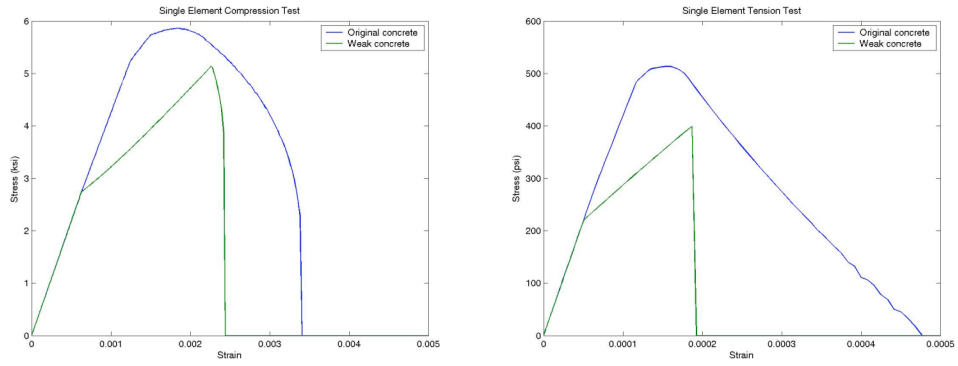

Figure 15. Stress-strain curves for a single element in unconfined compression (left) and unconfined tension (right) for the original and weak concrete models

With no rebar, the simulated roof displacement still underestimates the measured displacement (Figure 16). The model underestimates the experiment for all four ground motions. However, while the model starts out too stiff during the first earthquake, the stiffness of the model approaches the stiffness of the actual structure by the fourth earthquake (Figure 17). Since there is no rebar, the structure is highly damaged by the end of the fourth earthquake. The extent of damage is illustrated in Figure 18.

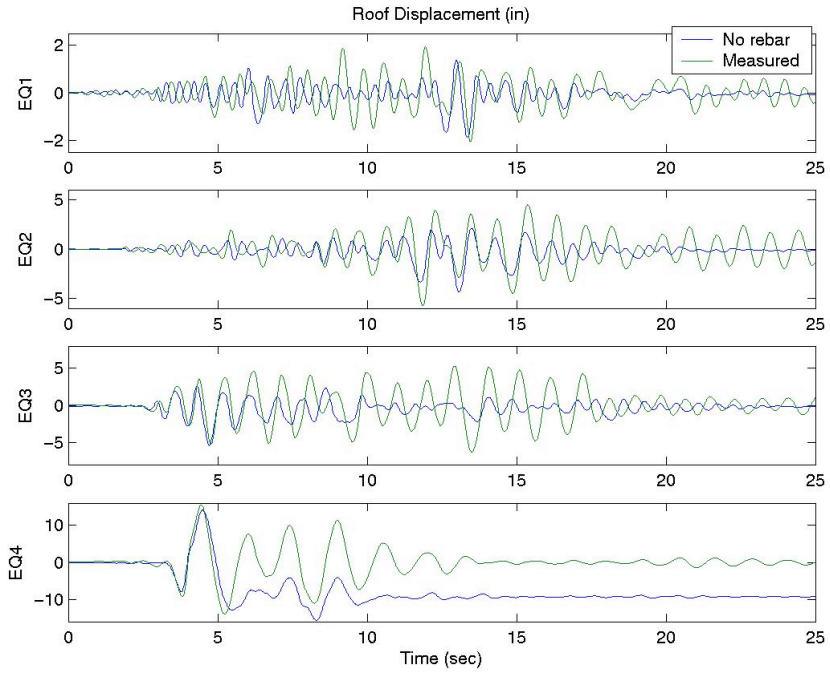

Figure 16. Roof displacements computed from the nonlinear model with no rebar for four earthquake ground motions compared to the measured roof displacements

Similarly with weaker concrete, the simulated displacement underestimates the measured displacement (Figure 19), and the model is initially too stiff. However, by the fourth earthquake, the model is damaged to such a high degree that the model is softer than the actual structure. Frequency response curves illustrating this are shown in Figure 20, and Figure 18 shows the damage sustained by the model. The fact that the damage is more severe with weaker concrete and rebar included than with the original concrete and no rebar demonstrates that the original concrete is probably too strong.

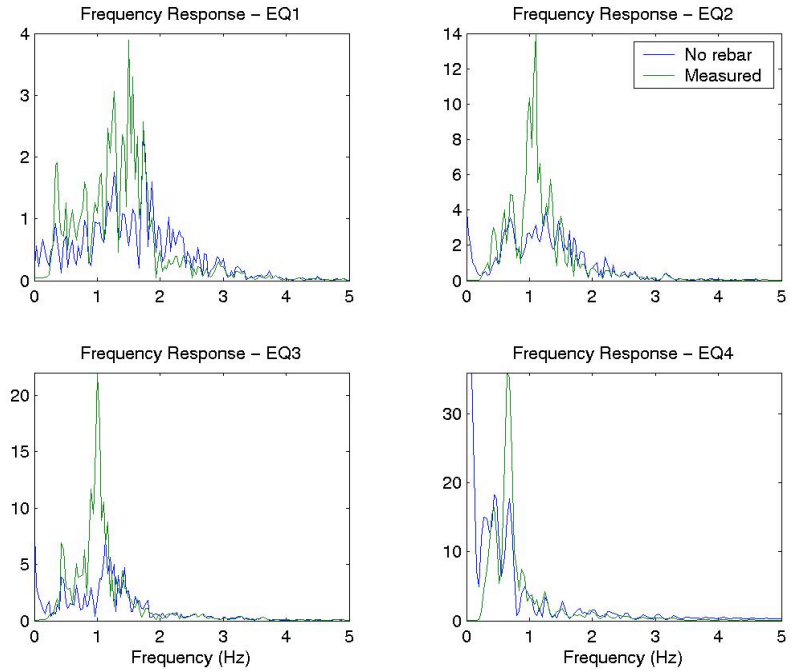

Figure 17. Frequency response curves of the roof displacements computed from the nonlinear model with no rebar for four earthquakes compared to the frequency responses of the measured roof displacements

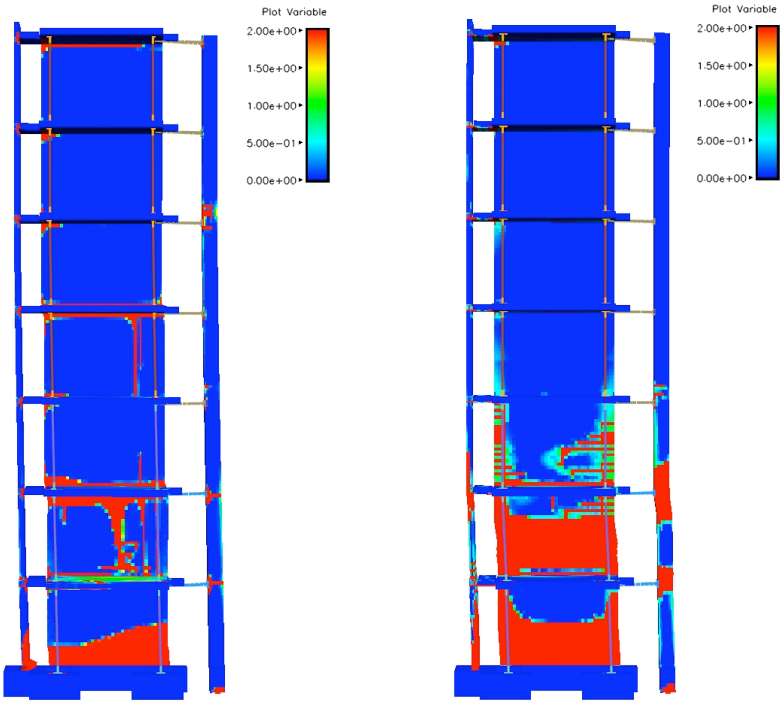

Figure 18. Plot of the concrete damage parameter throughout the nonlinear model with no rebar (left) and with weak concrete (right) at the end of the fourth earthquake

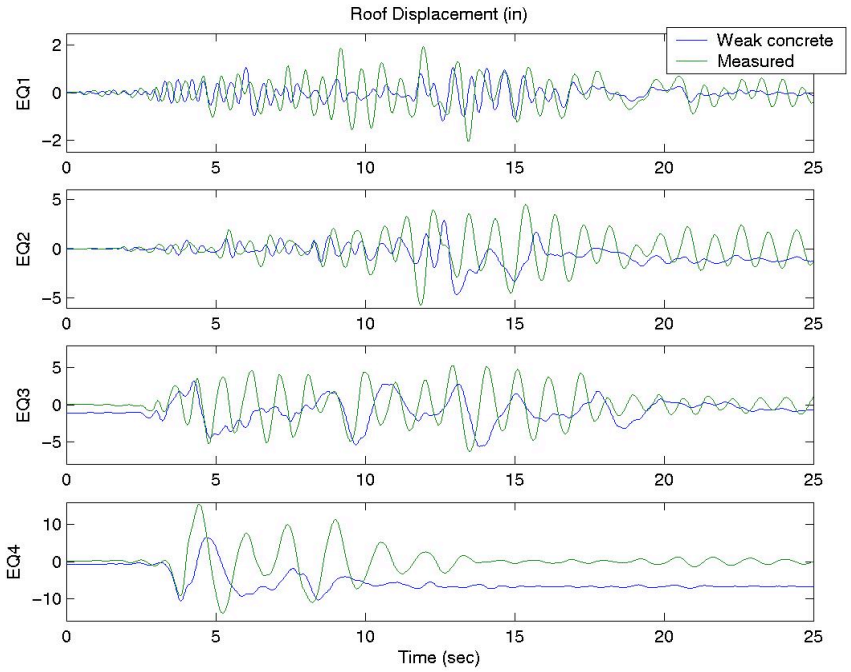

Figure 19. Roof displacements computed from the nonlinear model with weak concrete for four earthquake ground motions compared to the measured roof displacements

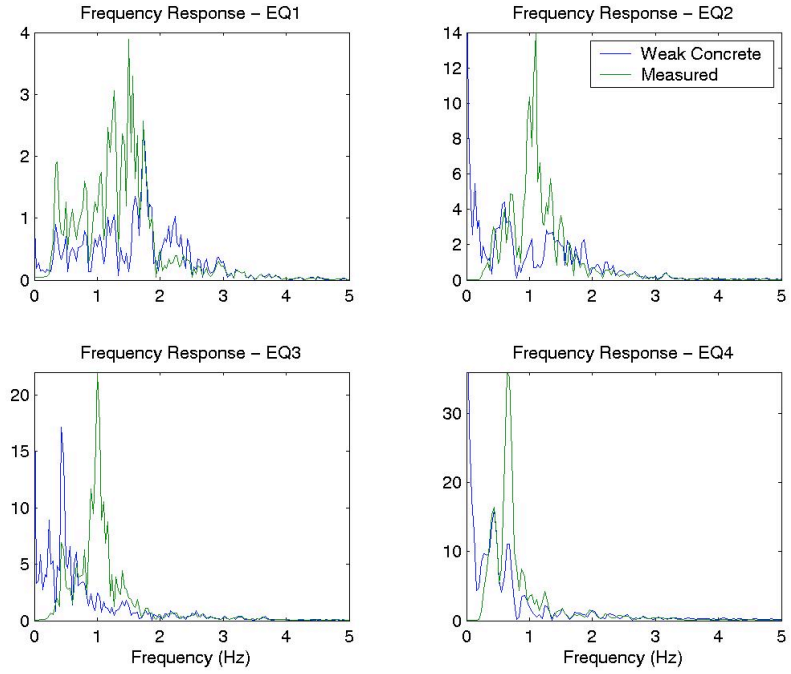

Figure 20. Frequency response curves of the roof displacements computed from the nonlinear model with weak concrete for four earthquakes compared to the frequency responses of the measured roof displacements

The effect of removing the damping is illustrated in Figure 21. While the effect is not negligible, it does not account for enough of a difference to explain the discrepancy in the simulated and measured responses. It is quite possible, however, that the assumed level of damping was too high at 3% of critical at 2.6 Hz, especially because mass proportional damping increases with decreasing frequency. This means that the damping is above 3% at frequencies below 2 Hz, which is where the actual structure predominantly oscillated.

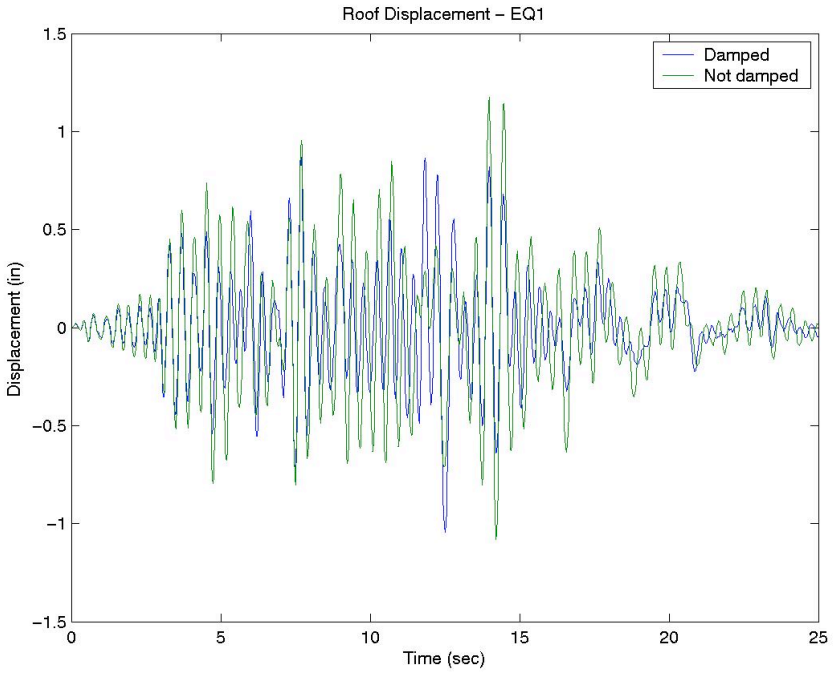

Figure 21. Comparison of the roof displacement computed for the first earthquake with damping and without damping included in the model

4.2.5 Wall Tests

In order to verify that the homogenized rebar model does not cause a significant increase in the stiffness of the building, a typical level of the web wall is generated with the homogenized rebar model and with explicit beam elements to model the rebar. Both of these models are used in ParaDyn analyses with simple load cases. Validation tests have been previously performed with the homogenized model, but the tests described here provide a simple comparison for a wall that uses the specific discretization employed for this suite of analyses.

The finite element mesh of the wall is illustrated in Figure 22, and the beam element representation of the rebar and the homogenized rebar discretization are illustrated in Figure 23. Tests were performed where the wall was pushed over in bending (x-direction) and in shear (y-direction), and put in tension and compression (z-direction). In all four loading cases, both models of the wall behave almost identically up to the point where there is significant nonlinearity in the concrete. This verifies that modeling with homogenized rebar yields the same initial stiffness as modeling with explicit beam elements. Force versus displacement curves for

the node at the center of the top of the wall are shown in Figure 24. Contour plots of the pertinent displacement for each of the cases are shown for the explicit beam model and the homogenized rebar model in Figure 25 through Figure 28.

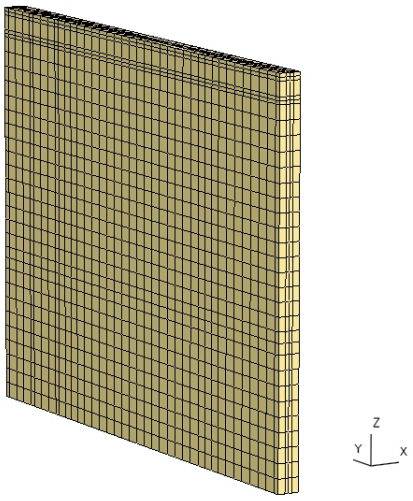

Figure 22. Finite element mesh of typical level of the web wall

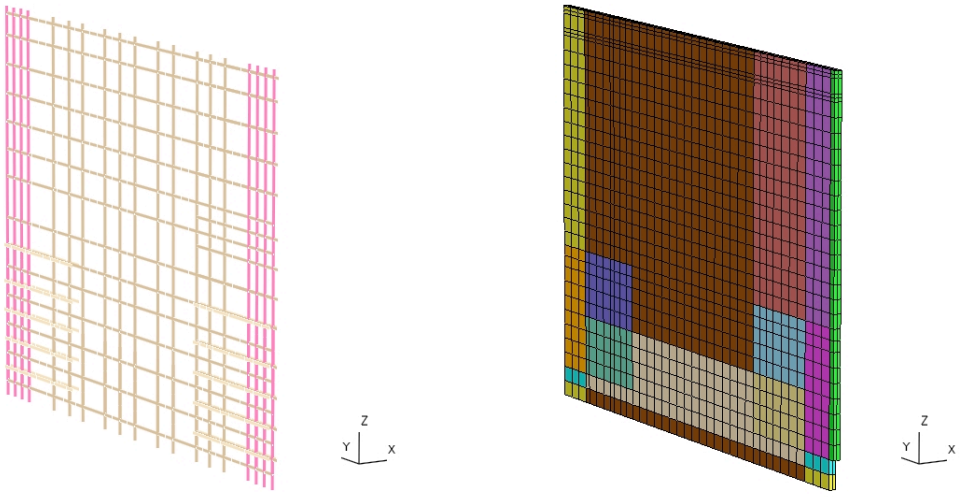

Figure 23. Beam element representation (left) and homogenized rebar representation (right) of the rebar in the web wall

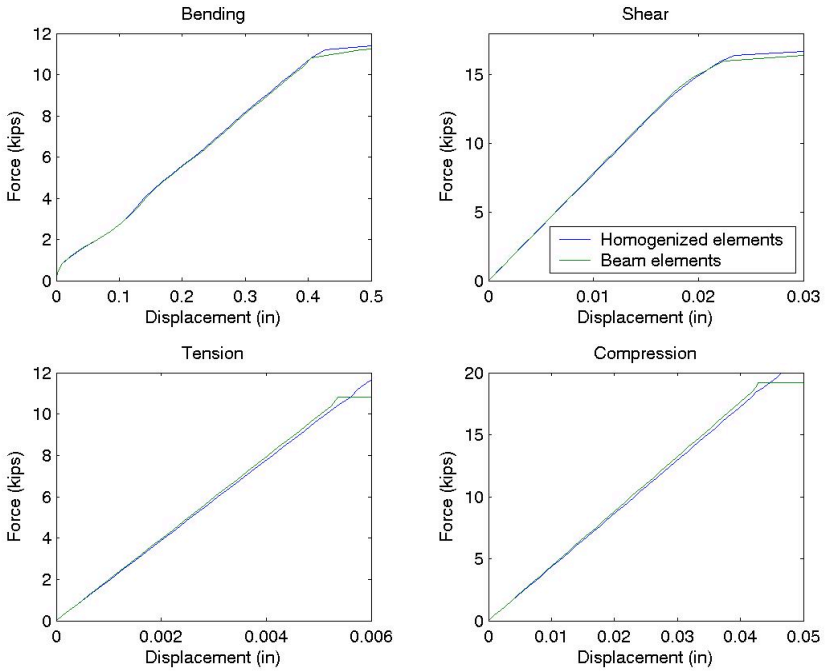

Figure 24. Force versus displacement (node 3448) for bending, shear, tension and compression tests of the web wall modeled with beam elements and homogenized rebar

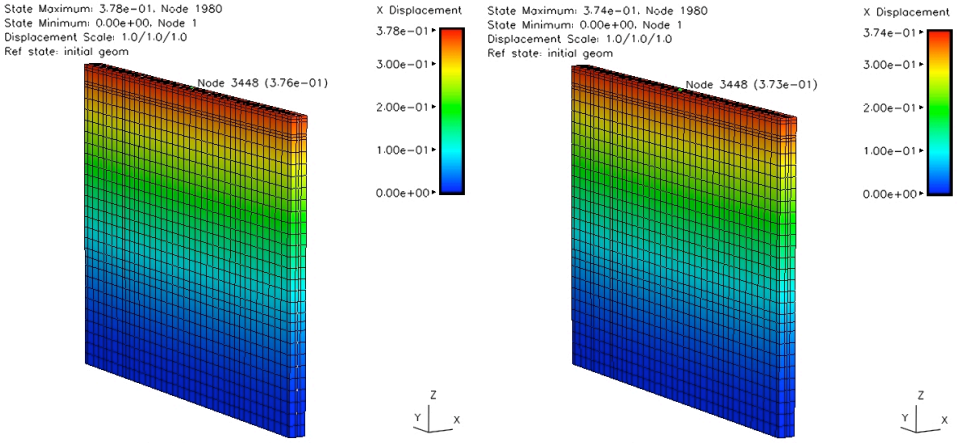

Figure 25. Contour plots of x-displacement for the bending test of the web wall modeled with beam elements (left) and homogenized rebar (right)

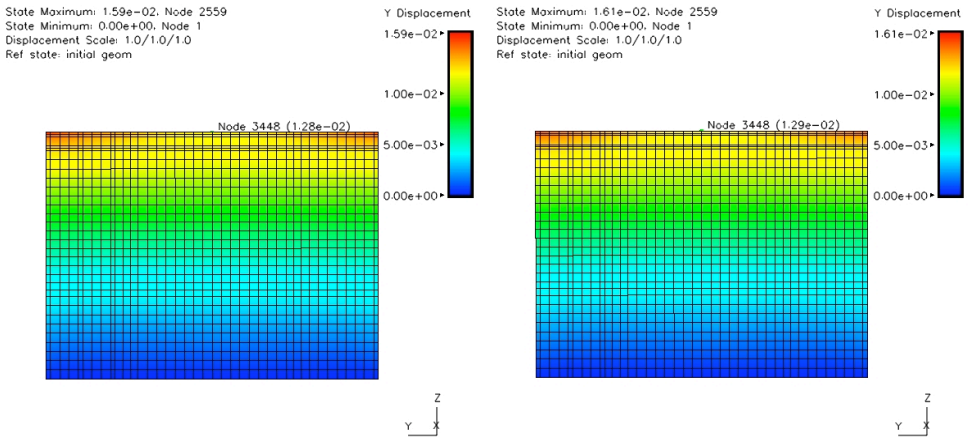

Figure 26. Contour plots of y-displacement for the shear test of the web wall modeled with beam elements (left) and homogenized rebar (right)

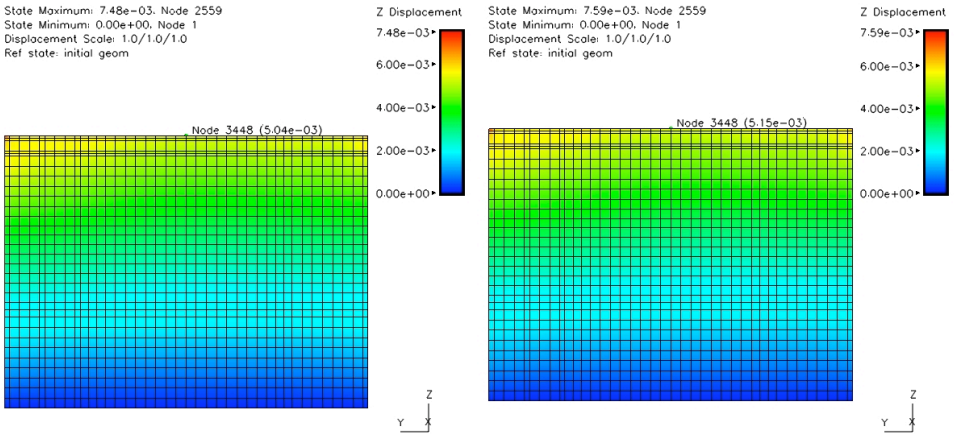

Figure 27. Contour plots of z-displacement for the tension test of the web wall modeled with beam elements (left) and homogenized rebar (right)

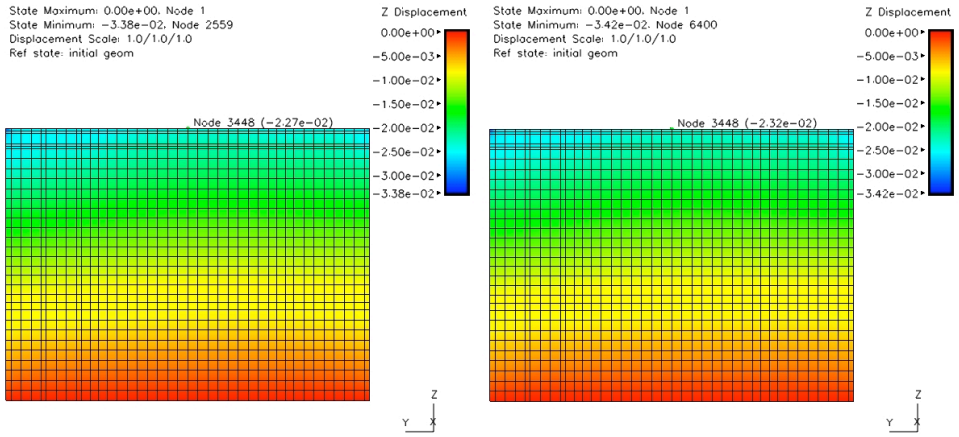

Figure 28. Contour plots of z-displacement for the compression test of the web wall modeled with beam elements (left) and homogenized rebar (right)

5.0 Possible Reasons for Discrepancies

Basically, the discrepancies between the simulated and measured responses are related to inaccuracies in the stiffness and mass of the system. The measured response of the structure shows larger displacements oscillating at lower frequencies than the model predicts. This means that the stiffness of the model is too high and/or the mass of the model is too low.

There are several possible reasons for the overestimation of stiffness. As previously mentioned, the concrete in the structure may have already been in a significant state of damage prior to the shaking with the first earthquake motion. Substantial concrete cracking may have occurred due to settling and the excitation of low-amplitude white noise tests. Also, construction joints in the concrete may be important. More detailed information about the structure would be necessary to properly assess these effects. The actual stress-strain behavior of the concrete could also be important. UCSD provided the compressive strength and the elastic modulus of the concrete samples, but this leaves a lot of freedom to define the stress versus strain relationship of the concrete. It is believed that the concrete properties generated by material type 65 of DYNA3D using compressive strength provide a stronger material than the actual concrete present in the structure. The assumption that the average concrete properties could be applied throughout the entire structure may also be contributing to the inaccuracy in stiffness. Notice from Table 1 and Figure 2 that the concrete in the first two levels of the structure had lower compressive strengths and elastic moduli than the other levels. Including this feature, along with better knowledge of the stress-strain behavior of each sample, would probably lead to better agreement with the experiment.

The gravity columns and braces are other possible sources of extra stiffness. The assumption of fixed connections and neglecting slackness at the ends of the columns (and braces, only during the fourth earthquake) adds some stiffness. However, the overall effect of these assumptions is expected to be small based on results discussed in Section 3.0 indicating that the gravity columns and braces do not contribute significantly to the stiffness of the structure.

The mass of the structure may be another important source of uncertainty. If the mass of the model is too low, the simulations will oscillate at higher frequencies. If there was a substantial lumped mass at the top floor of the structure, then this might help explain why the simulation underestimates the roof deflection. In order to decrease the frequency of the first cantilever mode of the structure enough to account for the discrepancy shown in Figure 12, the mass needs to be increased much more than would seem to be reasonable (see Section 3.0). Thus, while unknown mass may be a contributor to the discrepancies, it does not appear to dominate.

The models with no rebar and weaker concrete discussed in Section 4.2.4 show that even when the concrete is damaged to a significant degree, the simulation still underestimates the measured response at the roof. In both cases, the stiffness of the model does appear to be close to the actual structure by the fourth earthquake. One more possible reason for the underestimation, even at the fourth earthquake for these two models, is that the damping is too high in the model. As shown in Section 4.2.4, this does not appear to be that significant for the first earthquake, but since the model damping is mass proportional the amount of damping is higher at lower

frequencies. Thus, the damping may have an increasing impact as the four earthquake simulation progresses and the extent of concrete damage grows.

In order to validate the use of DYNA3D/ParaDyn and the DTRA concrete model with homogenized rebar for seismic simulations, more work is necessary. The singularity in the concrete model discussed in Section 4.2.2 needs to be investigated and dealt with. This may require modifications to the finite element code, or it may only require modifications to the concrete parameters that are provided as input. More importantly, the physical discrepancies between the experimental structure and the computational model need to be identified. Thus, more detailed information regarding the characteristics of the experimental structure is required from UCSD.

6.0 Acknowledgements

We would like to thank UC San Diego for providing information about the structure and results of the experiment.

7.0 References

1. Lin, J.I. DYNA3D: A Nonlinear, Explicit, Three-Dimensional Finite Element Code for Solid and Structural Mechanics, User Manual. Lawrence Livermore National Laboratory. Report UCRL-MA-107254, June 2005.
2. Hoover, C.G., A.J. De Groot, and R.J. Sherwood. ParaDyn User Manual, ParaDyn: A Parallel Nonlinear Explicit, Three-Dimensional Finite-Element Code for Solid and Structural Mechanics. Lawrence Livermore National Laboratory. Report UCRL-MA-140943-revised, January 2004.
3. Noble, C., E. Kokko, I. Darnell, T. Dunn, L. Hagler, and L. Leininger. Concrete Model Descriptions and Summary of Benchmark Studies for Blast Effects Simulations. Lawrence Livermore National Laboratory. Report UCRL-TR-215024, July 2005.
4. Puso, M.A., B.N. Maker, R.M. Ferencz, and J.O. Hallquist. NIKE3D, A Nonlinear, Implicit, Three-Dimensional Finite Element Code for Solid and Structural Mechanics, User's Manual. Lawrence Livermore National Laboratory. Report UCRL-MA-105268 Rev. 1, June 2004.